EDGE ARTICLE

Check for updates

Local electric field in nanocavities dictates the vibrational relaxation dynamics of interfacial molecules†

Xiaoxuan Zheng, [ID] [a] Quanbing Pei,[a] Junjun Tan,*[b] Shiyu Bai,[a] Yi Luo [ID] *[ab] and Shuji Ye [ID] *[ab]

Plasmonic nanocavities enable the generation of strong light–matter coupling and exhibit great potential in plasmon-mediated chemical reactions (PMCRs). Although an electric field generated by nanocavities (E_n) has recently been reported, its effect on the vibrational energy relaxation (VER) of the molecules in the nanocavities has not been explored. In this study, we reveal the impact of an electric field sensed by molecules (*para*-substituted thiophenol derivatives) in a nanocavity (E_f) on VER processes by employing advanced time-resolved femtosecond sum frequency generation vibrational spectroscopy (SFG-VS) supplemented by electrochemical measurements. The magnitude of E_n is almost identical (1.0 ± 0.2 V nm^{-1}) beyond the experimental deviation while E_f varies from 0.3 V nm^{-1} to 1.7 V nm^{-1} depending on the substituent. An exponential correlation between E_f and the complete recovery time of the ground vibrational C═C state (T_2) of the phenyl ring is observed. Substances with a smaller T_2 are strongly correlated with the reported macroscopic chemical reactivity. This finding may aid in enriching the current understanding of PMCRs and highlights the possibility of regulating vibrational energy flow into desired reaction coordinates by using a local electric field.

Introduction

Plasmonic nanocavities allow the localization and concentration of light into subnanoscale volumes and enable the generation of strong light–matter coupling.[1–3] This exceptional ability provides a novel platform for access to biosensing, quantum chemistry and materials science.[4–7] In particular, plasmonic nanocavities have been demonstrated to exhibit promising applications in mediating chemical reactions.[8–10] In theory, vibrational energy relaxation (VER) is fundamentally important for chemical reaction dynamics owing to its intrinsic connection with energy dissipation at reaction active sites and chromophores, as well as its ability to govern reaction coordinates.[11–15] Although plasmon-mediated chemical reactions (PMCRs) have achieved important milestones,[16,17] the underlying effects of plasmons on the VER processes of interfacial molecules have largely not been explored.

Currently, several mechanisms for PMCRs have been proposed, including electromagnetic fields,[18] hot electrons

(holes) and heat generated by excited plasmons,[19–21] and static electric fields.[22–24] In the last mechanism, the nanocavity can generate a direct current (DC) electric field (E_n) to mediate chemical reactions.[25–29] Here, E_n is an electrostatic field resulting from the photoexcitation of metal nanoparticles which is sustained over the full course of chemical turnover, rather than the instantaneous electric field resulting from the electromagnetic field concentration provided by plasmon resonance.[26] Although a chemical potential contributed by plasmonic excitation was recently shown,[23,29,30] direct probing of the DC electric field and its influence on molecules in the nanocavity is rather challenging.[25,26,30] As a result, insight into the effect of plasmonic excitation on interfacial VER processes is poorly understood. In this study, we used self-assembled monolayers (SAMs) of *para*-substituted thiophenol derivatives on gold films and in plasmonic nanocavities as models and revealed the impact of the electric field sensed by the molecules in the nanocavity (E_f) on the VER processes. We determined the magnitudes of E_n and E_f by investigating the bandwidth of the C═C stretching mode ($\nu_{C═C}$) of the phenyl ring *via* femtosecond sum frequency generation vibrational spectroscopy (SFG-VS) supplemented by electrochemical measurements. Here, the probed molecules are located in nanocavities based on a nanoparticle-on-mirror (NPoM) approach (Fig. 1a) (labeled as NPoM-SAMs).[31,32] The selected aromatic thiols are well known to form good SAMs on metal surfaces and are widely adopted in photocatalysis and biomedicine.[33–37] The feasibility and

[a] Hefei National Research Center for Physical Sciences at the Microscale, Department of Chemical Physics, University of Science and Technology of China, Hefei, Anhui, 230026, China. E-mail: yiluo@ustc.edu.cn; shujiye@ustc.edu.cn

[b] Hefei National Laboratory, University of Science and Technology of China, Hefei, Anhui, 230088, China. E-mail: jjtan@ustc.edu.cn

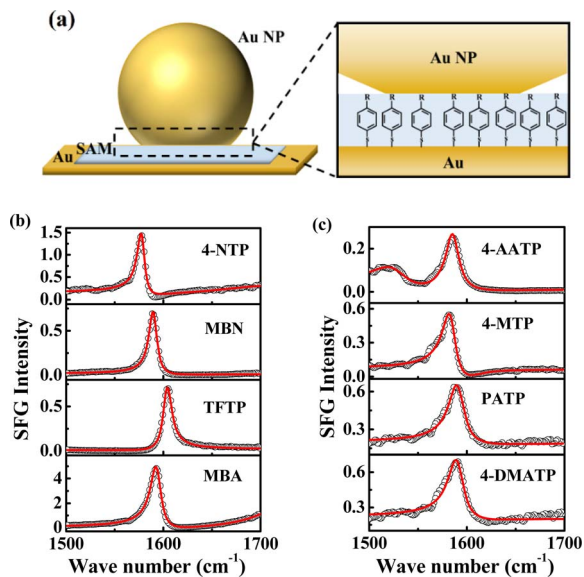† Electronic supplementary information (ESI) available. See DOI: https://doi.org/10.1039/d4sc02463j

Fig. 1 (a) Picture depicting the SAMs assembled in NPoMs, R = NO$_2$/CN/CF$_3$/COOH/NHCOCH$_3$/OCH$_3$/NH$_2$/N(CH$_3$)$_2$. The abbreviations for the corresponding substances are 4-NTP, MBN, TFTP, MBA, 4-AATP, 4-MTP, PATP and 4-DMATP. (b) The SE-SFG spectra of 4-NTP, MBN, TFTP and MBA in the frequency range of 1500–1700 cm^{-1}. (c) The SE-SFG spectra of 4-AATP, 4-MTP, PATP and 4-DMATP in the frequency range of 1500–1700 cm^{-1}.

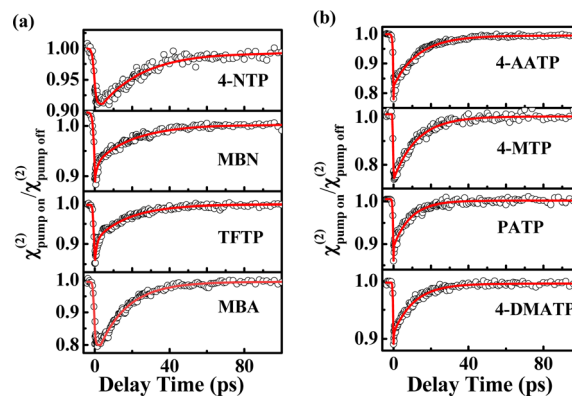
Fig. 2 (a) $\chi^{(2)}$ decay of the $\nu_{C=C}$ mode of the phenyl rings of 4-NTP, MBN, TFTP and MBA. (b) $\chi^{(2)}$ decay of the $\nu_{C=C}$ mode of the phenyl rings of 4-AATP, 4-MTP, PATP and 4-DMATP.

superiority of using the C=C stretching mode of the phenyl ring as a probe have been confirmed by surface-enhanced Raman spectroscopy (SERS).[38,39] E_n is approximately 1.0 ± 0.2 V nm^{-1}, and E_f varies from 0.3 V nm^{-1} to 1.7 V nm^{-1}. An exponential correlation between E_f and the complete recovery time of the ground vibrational C=C state (T_2) was observed. A substance with a smaller T_2 shows a strong correlation with the macroscopic chemical reactivity and plasmon-molecule interactions reported for PMCRs.[40,41] This work highlights the possibility of regulating vibrational energy flow into desired reaction coordinates using the local electric field in which the molecules are sensed in nanocavities. In addition, it is well known that local electric field strengths on the order of 1 V nm^{-1} are not only responsible for the vibrational Stark effect in both single-molecule systems[42] and condensed phases,[43] but can also selectively promote, drive, and control chemical reactions[44] such as proton transfer[45] and catalytic processes,[46–49] for example, the catalytic synthesis of ammonia from nitrogen and water microdroplets.[50,51] Therefore, the findings in this work may aid in enriching the current understanding of these processes including vibrational dynamics and catalytic processes.

Results and discussion

The ultrafast vibrational dynamics of the C=C stretching mode of NPoM-SAMs

We first measured the spectra and ultrafast vibrational dynamics of the $\nu_{C=C}$ mode of NPoM-SAMs using femtosecond time-resolved IR pump-SFG probe measurements. Fig. 1b and c

show the ppp spectra of the NPoM-SAMs in the frequency range of 1500–1700 cm^{-1}. All the peaks indicate a positive phase. The spectra in the frequency range of 1200–1800 cm^{-1} are displayed in Fig. S1.† All the samples had a $\nu_{C=C}$ frequency of 1585 ($\pm$15) cm^{-1}. Compared to those of the samples on the gold film without NPoMs (labeled as Au-SAMs) (Fig. S2†), the resonance signals of the molecules on the NPoM-SAMs are amplified with an enhancement factor >10^3. Fig. 2a and b depict the decay in the effective SFG peak strength ($\chi^{(2)}$) of the $\nu_{C=C}$ mode of thiophenol derivatives. In theory, SFG probes the surface population density of a vibrational state.[52,53] The excitation of $\nu_{C=C}$ from the ground state (ν_0) to its first vibrational state (ν_1) can reduce the SFG intensity. In general, the efficiency of vibrational excitation at the interface is very low. Currently, vibrational dynamics of only a few groups, such as OH and amide modes, have been reported.[52,54–56] In the absence of nanocavities, the bleaching value is too small to be detected (Fig. S3†). However, in the presence of nanocavities, clear bleaching following excitation at 1580 cm^{-1} at $t = 0$ was observed (Fig. 2a and b) due to plasmon-enhanced vibrational excitation.[57,58] Following this bleaching, the ν_1 state relaxes to an intermediate state, and the SFG intensity gradually recovers. The vibrational dynamics of the $\nu_{C=C}$ mode exhibit biexponential decays with a fast component (T_1) and a slow component (T_2). These two components were attributed to the fast population transfer between different C=C modes (T_1) and the slow complete recovery of the ground vibrational state (T_2), respectively. T_2 is dominated by a combination of intramolecular vibrational relaxation (IVR) and nonadiabatic relaxation which contributes to the excitation of electron–hole pairs (EHPs) in gold substrates and gold nanoparticles.[59,60] EHPs have been proven to be the primary energy transfer channel on metal surfaces.[61,62] The T_1 values of the different thiophenol derivatives are essentially identical at approximately 1 ps, which is consistent with the time required for rapid energy equilibrium among the delocalized $\nu_{C=C}$ modes.[63] In contrast, significant differences in T_2 values were observed across the samples (Table S1†). Specifically, the T_2 values are 21.4 ($\pm$1.3), 20.0 ($\pm$0.4), 17.3 ($\pm$0.5), 15.2 ($\pm$0.3), 13.8 ($\pm$0.4), 12.7 ($\pm$0.5), 9.7 ($\pm$0.7) and 10.4 ($\pm$1.4) ps for

4-NTP, MBN, TFTP, MBA, 4-AATP, 4-MTP, PATP and 4-DMATP, respectively. The difference in T_2 may arise from various factors, such as intermolecular interactions, molecular orientation, and the electric field.[64–66] The studied SAMs exhibit very similar orientations with respect to the metal surface, thus ruling out orientation as the main reason for the difference in T_2.[64] The effect of intermolecular interactions on T_2 can also be ruled out. Earlier reports suggested that the value of T_2 is strongly dependent on the π–π interactions between molecules, with stronger intermolecular interactions promoting faster molecular energy dissipation.[64] However, the observed results contradict this hypothesis. For instance, 4-NTP, which was expected to have a faster T_2 due to its strong π–π interaction, actually exhibited a longer T_2 (21.4 (±1.3) ps). Similarly, the presence of a –CF$_3$ group theoretically weakens π–π interactions and may result in an increase in the T_2 of the phenyl ring. However, these speculations in terms of intermolecular interactions contrast with our findings. Therefore, the electric field is most likely a significant factor in regulating vibrational relaxation dynamics. To verify this conjecture, we measured the magnitudes of E_n and E_f based on the DC Stark effect on the bandwidth of the $\nu_{C=C}$ mode of the phenyl ring by combining SFG-VS and electrochemical measurements.

Determination of the magnitudes of the electric field E_n and E_f

In principle, E_f in nanocavities consists of two components, the molecular internal electric field (E_i) and E_n (eqn (1)). In the absence of nanocavities, $E_f = E_i$. It has been reported that E_i is linearly related to the Hammett constant (σ) of the *para*-substituted group on the chemical moiety.[67–69] For simplicity of analysis, the magnitude of E_i in this work is the relative magnitude compared to that at $\sigma = 0$. Earlier studies indicated that the electric field can generate a vibrational Stark effect, yielding a linear correlation between the electric field and the frequency (ω)[70–73] or peak area (intensity)[74] of a vibrational mode. In addition to ω and peak area, the bandwidth also displays a linear dependence on the electric field and provides another molecular-level descriptor for evaluating the electric field (see eqn (2)–(4)).[67,75] To determine the magnitude of E_n, we

utilized an external electric potential (V) to increase the molecular bandwidth of the films in the absence of a nanocavity (Fig. 3a). When this bandwidth broadening of the "Au-SAMs + applied potential (V)" case equals the bandwidth broadening caused by the nanocavity, the value of the external electric potential can be used to determine the magnitude of the corresponding E_n using eqn (1)–(4). Specifically, by probing the $\nu_{C=C}$ bandwidth change of each Au-SAM at different applied potentials ($\Delta\Gamma_p$) using SFG-VS supplemented by electrochemical measurements, the dependence of $\Delta\Gamma_p$ on V can be determined by using eqn (2). The E_i and E_n of each sample can be deduced using eqn (3) and (4), respectively.

$$E_f = E_n + E_i \tag{1}$$

$$k^\sigma = \Delta\Gamma_p^\sigma / V \tag{2}$$

$$E_i = \left. \frac{\left(\Gamma_{Au}^\sigma - \Gamma_{Au}^{\sigma=0}\right)}{k^{\sigma=0}} \right/ d \tag{3}$$

$$E_n = \left. \frac{\left(\Gamma_{NPoM}^\sigma - \Gamma_{Au}^\sigma\right)}{k^\sigma} \right/ d \tag{4}$$

where k^σ is defined as the Stark bandwidth broadening rate, Γ_{Au}^σ is the bandwidth of the $\nu_{C=C}$ mode of thiophenol derivatives in the absence of nanocavities at zero applied electric potential, Γ_{NPoM}^σ is the corresponding bandwidth of the samples in the presence of nanocavities, and d is the spacer thickness of SAMs in the nanocavity. The subscript p represents the change induced by V, and the superscript σ corresponds to the Hammett constant. According to eqn (1)–(4), determining the values of E_n and E_f requires knowledge of Γ_{Au}^σ, Γ_{NPoM}^σ, and k^σ.

To determine the values of Γ_{Au}^σ and Γ_{NPoM}^σ, we fit the ppp spectra of the Au-SAMs and NPoM-SAMs (Fig. 1b, c and S2†) using a standard procedure (eqn (S1)†). The fitting parameters are shown in Tables S2 and S3.† The average Γ_{Au}^σ values were determined to be 4.1 (±0.4), 4.6 (±0.1), 5.1 (±0.4), 5.3 (±0.4), 6.2 (±0.5), 6.3 (±0.7), 7.2 (±0.3) and 7.7 (±0.6) cm^{-1} for 4-NTP, MBN, TFTP, MBA, 4-AATP, 4-MTP, PATP and 4-DMATP, respectively. The average Γ_{NPoM}^σ values were determined to be 4.6 (±0.2), 5.2 (±0.1), 5.8 (±0.2), 6.6 (±0.1), 8.2 (±0.6), 8.6 (±0.2), 11.2 (±0.3), and 12.1 (±0.5) cm^{-1} for 4-NTP, MBN, TFTP, MBA, 4-AATP, 4-MTP, PATP and 4-DMATP, respectively. The error bars represent more than 5 repeated experimental results (Tables S4 and S5†). The Hammett constants of the substituent groups in 4-NTP, MBN, TFTP, MBA, 4-AATP, 4-MTP, PATP and 4-DMATP are 0.78, 0.66, 0.54, 0.45, 0, −0.27, −0.66, and −0.83, respectively.[76] A good linear correlation between the bandwidth and Hammett constant is observed ($\Gamma_{Au}^\sigma = -2.0 \times \sigma + 5.9$ and $\Gamma_{NPoM}^\sigma = -4.3 \times \sigma + 8.1$) (Fig. 3b and c), indicating that the bandwidth can provide an effective descriptor for evaluating the electric field. Indeed, recent investigations on the carbonyl group of acetophenones have also demonstrated the linear dependence of the bandwidth on the Hammett constant[77] and potential.[67] Compared to those of Γ_{Au}^σ, the plot of Γ_{NPoM}^σ against the Hammett constant has a greater slope and intercept (Fig. 3b and c), revealing that the introduction of nanocavities
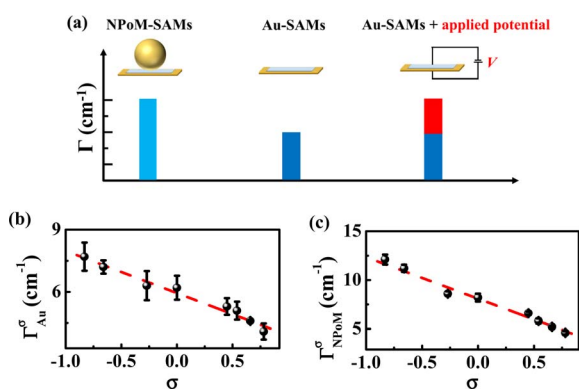

Fig. 3 (a) Schematic diagram for obtaining the magnitude of E_n based on the application of an external electric potential (V) to Au-SAMs. (b) Γ_{Au}^σ of Au-SAMs plotted against σ, and (c) Γ_{NPoM}^σ of NPoM-SAMs plotted against σ.

leads to peak broadening. Accordingly, the changes in bandwidth ($\Delta\Gamma_n = \Gamma_{NPoM}^\sigma - \Gamma_{Au}^\sigma$) in the absence and presence of nanocavities are 0.5 ($\pm$0.3), 0.6 ($\pm$0.1), 0.7 ($\pm$0.3), 1.3 ($\pm$0.4), 2.0 ($\pm$0.3), 2.3 ($\pm$0.7), 4.0 ($\pm$0.1), and 4.4 ($\pm$0.3) cm^{-1} for 4-NTP, MBN, TFTP, MBA, 4-AATP, 4-MTP, PATP and 4-DMATP, respectively. Theoretically, peak broadening can be caused by several factors, *e.g.*, pressure,[78] temperature,[79] and the electric field.[24,75,80,81] The effects of pressure and temperature can be excluded because the contributions caused by pressure and temperature are expected to be similar for different substituted groups with the same fluences of input laser pulses, which is opposite to what we have observed.

The value of k^σ can be determined by measuring the dependence of the bandwidth of the Au-SAMs (eqn (2)) on the potential *via* electrochemical testing experiments. Fig. 4a displays the potential-dependent SFG spectra of $\nu_{C=C}$ of MBN. The data for other Au-SAMs are provided in Fig. S4a.† Fig. 4b and S4b† depict the dependence of $\Delta\Gamma_p$ on V. As the potential increases, $\Delta\Gamma_p$ for MBN, 4-NTP, TFTP, MBA, 4-AATP, and 4-MTP linearly decreases (Fig. 4b and S4b†), while those for PATP and 4-DMATP linearly increase (Fig. S4b†). The values of k^σ are determined to be -0.5 ($\pm$0.1), -0.6 ($\pm$0.1), -0.9 ($\pm$0.1), -1.4 ($\pm$0.1), -2.0 ($\pm$0.1), -1.9 ($\pm$0.2), 4.0 ($\pm$0.4), and 4.4 ($\pm$0.9) cm^{-1} V^{-1} for 4-NTP, MBN, TFTP, MBA, 4-AATP, 4-MTP, PATP and 4-DMATP, respectively (Table S6†). Based on the linear relationship between k^σ and σ shown in Fig. S5,† $k^{\sigma=0}$ is deduced to be 2.2 cm^{-1} V^{-1}. With the assumption of $d \sim 1$ nm,[32,82,83] E_i is determined to be -0.7, -0.6, -0.5, -0.4, 0, 0.2, 0.6, and 0.7 V nm^{-1} for 4-NTP, MBN, TFTP, MBA, 4-AATP, 4-MTP, PATP, and 4-DMATP, respectively. Note that an electron withdrawing group (EWG) is equivalent to applying a negative electric field, while an electron donating group (EDG) represents the application of a positive electric field. This distinction arises from the fact that an upward electric field is defined as positive. When the substituent is an EWG, it induces an upward movement of the charge of the phenyl ring, equivalent to imposing a downward (negative) electric field.[68] In contrast, an EDG corresponds to
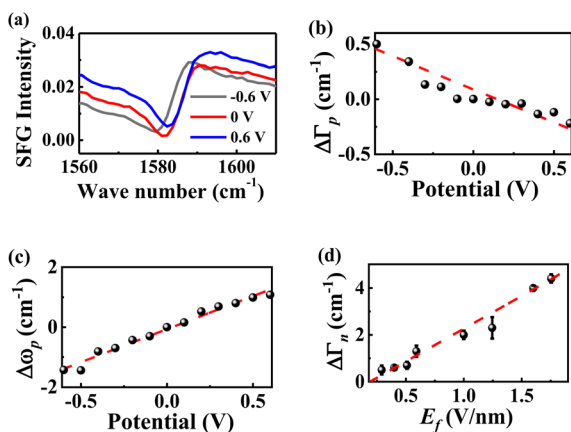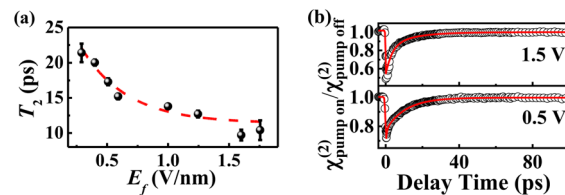

Fig. 5 (a) E_f plotted against the T_2 of thiophenol derivatives. (b) The ppp $\chi^{(2)}$ decay of the $\nu_{C=C}$ of 4-AATP at different potentials.

a positive electric field. Using eqn (4), E_n is deduced to be 1.0, 1.0, 0.8, 0.9, 1.0, 1.2, 1.0, and 1.0 V nm^{-1} for 4-NTP, MBN, TFTP, MBA, 4-AATP, 4-MTP, PATP, and 4-DMATP, respectively. The magnitude of E_n for all the studied samples is almost identical (1.0 $\pm$ 0.2 V nm^{-1}) beyond the experimental deviation. The magnitude of E_n can be further confirmed by the results determined using Stark shift (shown in the ESI†), which is an acknowledged tool for quantifying electric fields.[73,84] As a result, the E_f values of the different substituents were deduced to be 0.3, 0.4, 0.5, 0.6, 1.0, 1.2, 1.6 and 1.7 V nm^{-1} for 4-NTP, MBN, TFTP, MBA, 4-AATP, 4-MTP, PATP and 4-DMATP, respectively (Fig. 4d). The consistency of the electric field obtained through the peak shift and peak bandwidth provides robust support for the effectiveness of employing the bandwidth as a metric for electric field measurements.

The correlation between E_f and relaxation time T_2

We can now establish a correlation between E_f and T_2 (Fig. 5a). Evidently, T_2 exhibits an exponential dependence on E_f. A larger E_f corresponds to faster vibrational relaxation dynamics, while a smaller E_f corresponds to longer vibrational relaxation lifetimes. This correlation was further supported by the results obtained by applying a potential directly to 4-AATP (Fig. 5b). T_2 is 10.8 ps and 15.6 ps for $E_f = 1.5$ and 0.5 V nm^{-1}, respectively. E_f is related to the molecule–metal coupling. A larger E_f facilitates more efficient metal-molecule electron transfer and leads to faster transfer of molecular vibrational energy to the metal substrate, resulting in a shorter T_2. Accordingly, a substance with a smaller T_2 is expected to exhibit stronger reactivity because of its enhanced coupling to the metal. Indeed, this has been supported by some recent reports associated with PMCRs. For example, the H$_2$ production rate of 4-MTP in plasmon-mediated hydrogenolysis reactions was approximately 60 times greater than that of 4-NTP.[40] The plasmon-mediated methyl dehydrogenation occurrence rate of 4-methylbenzenethiol (4-MBT) exhibited a more than twofold increase at +0.5 V compared to that at −0.5 V.[41]

Conclusion

In this study, we utilized femtosecond broadband SFG to investigate the electric field sensed by the molecules in a nanocavity (E_f) and its impact on the ultrafast dynamics of *para*-substituted thiophenol molecules confined within nanocavities. We demonstrate that the magnitude of the electric field generated in the nanocavity (E_n) and E_f can be determined by

Fig. 4 (a) Potential-dependent SFG spectra of MBN between 0.6 V and −0.6 V *vs.* Ag/AgCl. $\Delta\Gamma_p$ (b) and $\Delta\omega_p$ (c) of $\nu_{C=C}$ of MBN as a function of the electric potential. (d) The $\Delta\Gamma_n$ values of thiophenol derivatives plotted against E_f.

investigating the bandwidth of the C≡C stretching mode of the phenyl ring by combining SFG-VS and electrochemical measurements. E_n is approximately 1.0 ± 0.2 V nm^{-1}. E_f is determined to be 0.3, 0.4, 0.5, 0.6, 1.0, 1.2, 1.6 and 1.7 V nm^{-1} for 4-NTP, MBN, TFTP, MBA, 4-AATP, 4-MTP, PATP and 4-DMATP, respectively. An exponential correlation between E_f and the complete recovery time of the ground vibrational C≡C state (T_2) is observed. By extending this correlation to the reported macroscopic chemical reactivity (k_{CR}), a profound connection between a higher k_{CR} and a smaller T_2 is found. This finding highlights the possibility of regulating vibrational energy flow into a desired reaction coordinate by introducing rationally designed molecular functionalities within spatially confined nanoscale environments. A molecular-level perspective on the relationship between k_{CR}, E_f and T_2 may aid in enriching the current understanding of PMCRs.

Methods

Materials and sample preparation

4-(Trifluoromethyl)-thiophenol (TFTP, with a purity >98%), 4-acetamidothiophenol (4-AATP, with a purity >95%) and 4-methoxythiophenol (4-MTP, with a purity >98%) were purchased from Shanghai Macklin Biochemical Technology Co., Ltd. 4-Nitrothiophenol (4-NTP, with a purity >95%) and p-aminothiophenol (PATP, with a purity >98%) were obtained from Aladdin. 4-Mercaptobenzonitrile (MBN, with a purity >97%) was obtained from Shanghai Haohong Scientific Co., Ltd. P-mercaptobenzoic acid (MBA, with a purity >90%) was purchased from Shanghai Acmec Biochemical Co., Ltd. 4-Dimethylamino-thiophenol (4-DMATP, with a purity >98%) was purchased from Shanghai Canspec S&T Co., Ltd. Ethanol and n-hexane were purchased from Sinopharm Chemical Reagent Co., Ltd. Ultrapure deionized (DI) water was purified by using a Milli-Q reference system. All the chemicals were used as received.

The substituents in 4-NTP, MBN, TFTP and MBA are EWGs –NO$_2$, –CN, –CF$_3$ and –COOH, respectively, while 4-AATP, 4-MTP, PATP and 4-DMATP are substituted with the EDGs –NHCOCH$_3$, –OCH$_3$, –NH$_2$ and –N(CH$_3$)$_2$, respectively. The specific sample preparation method is described in the ESI.†

SFG-VS experiments

All SFG experiments were carried out using a femtosecond time-resolved SFG-VS system. Detailed information about the instrument parameters was provided in our previous studies.[52,54] For a IR pump- SFG probe time-resolved SFG instrument, the pulse energies of the pump IR and probe IR pulses were ~12 μJ and 11 μJ at ~1580 cm^{-1}, respectively. The pulse energy of vis was 0.4 μJ. The specific spectral fitting procedures and data analysis have been presented in our publications[56,85] and are included in the ESI† for reference.

Electrochemical measurements

Electrochemical measurements were performed using a CHI660e workstation. The working electrode was a Au-SAM sample with a wire in contact with the Au film, the reference electrode was Ag/AgCl (in 3 M KCl), and the counter electrode was a Pt wire electrode. The electrolyte was a 0.3 M KCl solution. All potentials in the paper were relative to Ag/AgCl/3 M KCl, and a schematic diagram of the device is shown in Fig. S6.† *In situ* SFG measurements of Au-SAMs were performed over a potential range of −0.6 to 0.6 V to prevent desorption of thiol groups with a potential interval of 0.1 V. Fig. S7† illustrates the cyclic voltammetry curve with MBN as a typical example.

Data availability

The data that support the findings of this study are available from the corresponding author upon reasonable request.

Author contributions

X. X. Zheng: conceptualization, investigation, formal analysis, visualization, writing – original draft preparation, writing – reviewing and editing; Q. B. Pei: investigation, writing – reviewing and editing; J. J. Tan: software, funding acquisition, project administration, data curation, writing – reviewing and editing; S. Y. Bai: writing – reviewing and editing; Y. Luo: conceptualization, funding acquisition, manuscript drafting; S. J. Ye: conceptualization, funding acquisition, supervision, data analysis, manuscript drafting, writing – reviewing and editing.

Conflicts of interest

The authors declare no competing financial interest.

Acknowledgements

References

1 J. Sun, H. Hu, Y. Xu, Y. Li and H. Xu, Revealing the Photothermal Behavior of Plasmonic Gap Modes: Toward Thermostable Nanocavities, *Laser Photonics Rev.*, 2022, **16**, 2100564.

2 V. A. Milichko, D. A. Zuev, D. G. Baranov, G. P. Zograf, K. Volodina, A. A. Krasilin, I. S. Mukhin, P. A. Dmitriev, V. V. Vinogradov, S. V. Makarov and P. A. Belov, Metal-Dielectric Nanocavity for Real-Time Tracing Molecular Events with Temperature Feedback, *Laser Photonics Rev.*, 2018, **12**, 1700227.

3 C.-Y. Li, S. Duan, B.-Y. Wen, S.-B. Li, M. Kathiresan, L.-Q. Xie, S. Chen, J. R. Anema, B.-W. Mao, Y. Luo, Z.-Q. Tian and J.-F. Li, Observation of Inhomogeneous Plasmonic Field Distribution in a Nanocavity, *Nat. Nanotechnol.*, 2020, **15**, 922–926.

4 G. Huang, K. Liu, G. Shi, Q. Guo, X. Li, Z. Liu, W. Ma and T. Wang, Elevating Surface-Enhanced Infrared Absorption with Quantum Mechanical Effects of Plasmonic Nanocavities, *Nano Lett.*, 2022, **22**, 6083–6090.

5 E. Kokin, H. J. An, D. Koo, S. Han, K. Whang, T. Kang, I. Choi and L. P. Lee, Quantum Electrodynamic Behavior of Chlorophyll in a Plasmonic Nanocavity, *Nano Lett.*, 2022, **22**, 9861–9868.

6 A. Xomalis, R. Chikkaraddy, E. Oksenberg, I. Shlesinger, J. Huang, E. C. Garnett, A. F. Koenderink and J. J. Baumberg, Controlling Optically Driven Atomic Migration Using Crystal-Facet Control in Plasmonic Nanocavities, *ACS Nano*, 2020, **14**, 10562–10568.

7 A. Naldoni, V. M. Shalaev and M. L. Brongersma, Applying Plasmonics to a Sustainable Future, *Science*, 2017, **356**, 908–909.

8 B. S. Hoener, S. R. Kirchner, T. S. Heiderscheit, S. S. E. Collins, W.-S. Chang, S. Link and C. F. Landes, Plasmonic Sensing and Control of Single-Nanoparticle Electrochemistry, *Chem*, 2018, **4**, 1560–1585.

9 D. W. Kim and J.-W. Jang, Plasmonic Nanocavity as a Spectroscopic Probe for Molecules, *Matter*, 2022, **5**, 3102–3104.

10 E. Oksenberg, I. Shlesinger, A. Xomalis, A. Baldi, J. J. Baumberg, A. F. Koenderink and E. C. Garnett, Energy-Resolved Plasmonic Chemistry in Individual Nanoreactors, *Nat. Nanotechnol.*, 2021, **16**, 1378–1385.

11 J. Owrutsky, D. Raftery and R. Hochstrasser, Vibrational Relaxation Dynamics in Solutions, *Annu. Rev. Phys. Chem.*, 1994, **45**, 519–555.

12 F. F. Crim, Chemical Dynamics of Vibrationally Excited Molecules: Controlling Reactions in Gases and on Surfaces, *Proc. Natl. Acad. Sci. U.S.A.*, 2008, **105**, 12654–12661.

13 J. F. Cahoon, K. R. Sawyer, J. P. Schlegel and C. B. Harris, Determining Transition-State Geometries in Liquids Using 2D-IR, *Science*, 2008, **319**, 1820–1823.

14 L. Chuntonov, Using Mirrors to Control Molecular Dynamics, *Science*, 2022, **378**, 712.

15 R. Yin and B. Jiang, Mechanical Vibrational Relaxation of No Scattering from Metal and Insulator Surfaces: When and Why They Are Different, *Phys. Rev. Lett.*, 2021, **126**, 156101.

16 C. Zhan, J. Yi, S. Hu, X.-G. Zhang, D.-Y. Wu and Z.-Q. Tian, Plasmon-Mediated Chemical Reactions, *Nat. Rev. Dis. Primers*, 2023, **3**, 12.

17 E. Cortés, R. Grzeschik, S. A. Maier and S. Schlücker, Experimental Characterization Techniques for Plasmon-Assisted Chemistry, *Nat. Rev. Chem*, 2022, **6**, 259–274.

18 Z. Liu, W. Hou, P. Pavaskar, M. Aykol and S. B. Cronin, Plasmon Resonant Enhancement of Photocatalytic Water Splitting Under Visible Illumination, *Nano Lett.*, 2011, **11**, 1111–1116.

19 E. L. Keller and R. R. Frontiera, Ultrafast Nanoscale Raman Thermometry Proves Heating Is Not a Primary Mechanism for Plasmon-Driven Photocatalysis, *ACS Nano*, 2018, **12**, 5848–5855.

20 E. Kazuma, J. Jung, H. Ueba, M. Trenary and Y. Kim, Real-Space and Real-Time Observation of a Plasmon-Induced Chemical Reaction of a Single Molecule, *Science*, 2018, **360**, 521–526.

21 A. A. Golubev, B. N. Khlebtsov, R. D. Rodriguez, Y. Chen and D. R. T. Zahn, Plasmonic Heating Plays a Dominant Role in the Plasmon-Induced Photocatalytic Reduction of 4-Nitrobenzenethiol, *J. Phys. Chem. C*, 2018, **122**, 5657–5663.

22 D. R. Ward, F. Hüser, F. Pauly, J. C. Cuevas and D. Natelson, Optical Rectification and Field Enhancement in a Plasmonic Nanogap, *Nat. Nanotechnol.*, 2010, **5**, 732–736.

23 D. Kos, D. R. Assumpcao, C. Guo and J. J. Baumberg, Quantum Tunneling Induced Optical Rectification and Plasmon-Enhanced Photocurrent in Nanocavity Molecular Junctions, *ACS Nano*, 2021, **15**, 14535–14543.

24 H. Wang, K. Yao, J. A. Parkhill and Z. D. Schultz, Detection of Electron Tunneling across Plasmonic Nanoparticle–Film Junctions Using Nitrile Vibrations, *Phys. Chem. Chem. Phys.*, 2017, **19**, 5786–5796.

25 S. Yu and P. K. Jain, The Chemical Potential of Plasmonic Excitations, *Angew. Chem., Int. Ed.*, 2020, **59**, 2085–2088.

26 A. J. Wilson and P. K. Jain, Light-Induced Voltages in Catalysis by Plasmonic Nanostructures, *Acc. Chem. Res.*, 2020, **53**, 1773–1781.

27 D. A. Nelson and Z. D. Schultz, Influence of Optically Rectified Electric Fields on the Plasmonic Photocatalysis of 4-Nitrothiophenol and 4-Aminothiophenol to 4,4-Dimercaptoazobenzene, *J. Phys. Chem. C*, 2018, **122**, 8581–8588.

28 D. A. Nelson and Z. D. Schultz, The Impact of Optically Rectified Fields on Plasmonic Electrocatalysis, *Faraday Discuss.*, 2019, **214**, 465–477.

29 D. A. Nelson and Z. D. Schultz, Impact of Plasmon-Induced Optically Rectified Electric Fields on Second Harmonic Generation, *J. Phys. Chem. C*, 2019, **123**, 20639–20648.

30 M. T. Sheldon, J. van de Groep, A. M. Brown, A. Polman and H. A. Atwater, Plasmoelectric Potentials in Metal Nanostructures, *Science*, 2014, **346**, 828–831.

31 A. Ahmed, K. Banjac, S. S. Verlekar, F. P. Cometto, M. Lingenfelder and C. Galland, Structural Order of the Molecular Adlayer Impacts the Stability of Nanoparticle-on-Mirror Plasmonic Cavities, *ACS Photonics*, 2021, **8**, 1863–1872.

32 J. J. Baumberg, J. Aizpurua, M. H. Mikkelsen and D. R. Smith, Extreme Nanophotonics from Ultrathin Metallic Gaps, *Nat. Mater.*, 2019, **18**, 668–678.

33 N. S. Mueller, R. Arul, L. A. Jakob, M. O. Blunt, T. Földes, E. Rosta and J. J. Baumberg, Collective Mid-Infrared Vibrations in Surface-Enhanced Raman Scattering, *Nano Lett.*, 2022, **22**, 7254–7260.

34 F. M. M. Aldosari, Characterization of Labeled Gold Nanoparticles for Surface-Enhanced Raman Scattering, *Molecules*, 2022, **27**, 892.

35 R. D. Norton, H. T. Phan, S. N. Gibbons and A. J. Haes, Quantitative Surface-Enhanced Spectroscopy, *Annu. Rev. Phys. Chem.*, 2022, **73**, 141–162.

36 L. Dong, X. Yang, C. Zhang, B. Cerjan, L. Zhou, M. L. Tseng, Y. Zhang, A. Alabastri, P. Nordlander and N. J. Halas, Nanogapped Au Antennas for Ultrasensitive Surface-Enhanced Infrared Absorption Spectroscopy, *Nano Lett.*, 2017, **17**, 5768–5774.

37 K. Chen and H. Wang, Plasmon-Driven Photocatalytic Molecular Transformations on Metallic Nanostructure Surfaces: Mechanistic Insights Gained from Plasmon-Enhanced Raman Spectroscopy, *Mol. Syst. Des. Eng.*, 2021, **6**, 250–280.

38 S. Hati, X. Yang, P. Gupta, B. B. Muhoberac, J. Pu, J. Zhang and R. Sardar, Hybrid Metal-Ligand Interfacial Dipole Engineering of Functional Plasmonic Nanostructures for Extraordinary Responses of Optoelectronic Properties, *ACS Nano*, 2023, **17**, 17499–17515.

39 B. C. Pein, N.-H. Seong and D. D. Dlott, Vibrational Energy Relaxation of Liquid Aryl-Halides X-C_6H_5 (X = F, Cl, Br, I), *J. Phys. Chem. A*, 2010, **114**, 10500–10507.

40 G. Joshi, R. Kashyap, K. Patrikar, A. Mondal and S. Khatua, Ligand-Mediated Electron Transport Channels Enhance Photocatalytic Activity of Plasmonic Nanoparticles, *Nanoscale*, 2023, **15**, 16552–16560.

41 J. Zhou, J. Guo, G. Ghimire, A. M. Mebel, S. Chang and J. He, Plasmon-Mediated Dehydrogenation of the Aromatic Methyl Group and Benzyl Radical Formation, *Chem. Sci.*, 2023, **14**, 13951–13961.

42 V. Mollica Nardo, G. Cassone, R. C. Ponterio, F. Saija, J. Sponer, M. Tommasini and S. Trusso, Electric-Field-Induced Effects on the Dipole Moment and Vibrational Modes of the Centrosymmetric Indigo Molecule, *J. Phys. Chem. A*, 2020, **124**, 10856–10869.

43 G. Cassone, J. Sponer, S. Trusso and F. Saija, Ab Initio Spectroscopy of Water under Electric Fields, *Phys. Chem. Chem. Phys.*, 2019, **21**, 21205–21212.

44 A. C. Aragonès, N. L. Haworth, N. Darwish, S. Ciampi, N. J. Bloomfield, G. G. Wallace, I. Diez-Perez and M. L. Coote, Electrostatic Catalysis of a Diels–Alder Reaction, *Nature*, 2016, **531**, 88–91.

45 G. Cassone, Nuclear Quantum Effects Largely Influence Molecular Dissociation and Proton Transfer in Liquid Water under an Electric Field, *J. Phys. Chem. Lett.*, 2020, **11**, 8983–8988.

46 F. Che, J. T. Gray, S. Ha, N. Kruse, S. L. Scott and J.-S. McEwen, Elucidating the Roles of Electric Fields in Catalysis: A Perspective, *ACS Catal.*, 2018, **8**, 5153–5174.

47 S. Shaik, D. Mandal and R. Ramanan, Oriented Electric Fields as Future Smart Reagents in Chemistry, *Nat. Chem.*, 2016, **8**, 1091–1098.

48 G. Cassone, J. Sponer and F. Saija, Ab Initio Molecular Dynamics Studies of the Electric-Field-Induced Catalytic Effects on Liquids, *Top. Catal.*, 2022, **65**, 40–58.

49 G. Cassone, F. Pietrucci, F. Saija, F. Guyot and A. M. Saitta, One-Step Electric-Field Driven Methane and Formaldehyde Synthesis from Liquid Methanol, *Chem. Sci.*, 2017, **8**, 2329–2336.

50 X. Song, C. Basheer and R. N. Zare, Making Ammonia from Nitrogen and Water Microdroplets, *Proc. Natl. Acad. Sci. U.S.A.*, 2023, **120**, e2301206120.

51 G. Cassone, F. Saija, J. Sponer and S. Shaik, The Reactivity-Enhancing Role of Water Clusters in Ammonia Aqueous Solutions, *J. Phys. Chem. Lett.*, 2023, **14**, 7808–7813.

52 J. J. Tan, B. X. Zhang, Y. Luo and S. J. Ye, Ultrafast Vibrational Dynamics of Membrane-Bound Peptides at the Lipid Bilayer/Water Interface, *Angew. Chem., Int. Ed.*, 2017, **56**, 12977–12981.

53 Y. R. Shen, *The Principles of Nonlinear Optics*, Wiley-Interscience, New York, NY, USA, United States, 1984.

54 J. J. Tan, J. H. Zhang, C. Z. Li, Y. Luo and S. J. Ye, Ultrafast Energy Relaxation Dynamics of Amide I Vibrations Coupled with Protein-Bound Water Molecules, *Nat. Commun.*, 2019, **10**, 1010.

55 S. Nihonyanagi, S. Yamaguchi and T. Tahara, Ultrafast Dynamics at Water Interfaces Studied by Vibrational Sum Frequency Generation Spectroscopy, *Chem. Rev.*, 2017, **117**, 10665–10693.

56 J. J. Tan, Z. J. Ni and S. J. Ye, Protein-Water Coupling Tunes the Anharmonicity of Amide I Modes in the Interfacial Membrane-Bound Proteins, *J. Chem. Phys.*, 2022, **156**, 105103.

57 I. Morichika, K. Murata, A. Sakurai, K. Ishii and S. Ashihara, Molecular Ground-State Dissociation in the Condensed Phase Employing Plasmonic Field Enhancement of Chirped Mid-Infrared Pulses, *Nat. Commun.*, 2019, **10**, 3893.

58 J. P. Kraack and P. Hamm, Vibrational Ladder-Climbing in Surface-Enhanced, Ultrafast Infrared Spectroscopy, *Phys. Chem. Chem. Phys.*, 2016, **18**, 16088–16093.

59 C. Anfuso, A. M. Ricks, W. Rodríguez-Córdoba and T. Lian, Ultrafast Vibrational Relaxation Dynamics of a Rhenium Bipyridyl CO_2-Reduction Catalyst at a Au Electrode Surface Probed by Time-Resolved Vibrational Sum Frequency Generation Spectroscopy, *J. Phys. Chem. C*, 2012, **116**, 26377–26384.

60 A. Ge, B. Rudshteyn, J. Zhu, R. J. Maurer, V. S. Batista and T. Lian, Electron-Hole-Pair-Induced Vibrational Energy Relaxation of Rhenium Catalysts on Gold Surfaces, *J. Phys. Chem. Lett.*, 2018, **9**, 406–412.

61 M. Askerka, R. J. Maurer, V. S. Batista and J. C. Tully, Role of Tensorial Electronic Friction in Energy Transfer at Metal Surfaces, *Phys. Rev. Lett.*, 2016, **116**, 217601.

62 H. Arnolds and M. Bonn, Ultrafast Surface Vibrational Dynamics, *Surf. Sci. Rep.*, 2010, **65**, 45–66.

63 X. He, P. Yu, J. Zhao and J. Wang, Efficient Vibrational Energy Transfer through Covalent Bond in Indigo Carmine Revealed by Nonlinear IR Spectroscopy, *J. Phys. Chem. B*, 2017, **121**, 9411–9421.

64 Z. Yu and R. R. Frontiera, Intermolecular Forces Dictate Vibrational Energy Transfer in Plasmonic-Molecule Systems, *ACS Nano*, 2022, **16**, 847–854.

65 C. Matranga and P. Guyot-Sionnest, Vibrational Relaxation of Cyanide at the Metal/Electrolyte Interface, *J. Chem. Phys.*, 2000, **112**, 7615–7621.

66 M. E. Schmidt and P. Guyot-Sionnest, Electrochemical Tuning of the Lifetime of the Co Stretching Vibration for Co/Pt(111), *J. Chem. Phys.*, 1996, **104**, 2438–2445.

67 S. D. Fried, L.-P. Wang, S. G. Boxer, P. Ren and V. S. Pande, Calculations of the Electric Fields in Liquid Solutions, *J. Phys. Chem. B*, 2013, **117**, 16236–16248.

68 S. Sarkar, J. G. Patrow, M. J. Voegtle, A. K. Pennathur and J. M. Dawlaty, Electrodes as Polarizing Functional Groups: Correlation between Hammett Parameters and Electrochemical Polarization, *J. Phys. Chem. C*, 2019, **123**, 4926–4937.

69 J. Heo, H. Ahn, J. Won, J. G. Son, H. K. Shon, T. G. Lee, S. W. Han and M.-H. Baik, Electro-Inductive Effect: Electrodes as Functional Groups with Tunable Electronic Properties, *Science*, 2020, **370**, 214–219.

70 S. Chen, Y.-H. Xiao, M. Qin, G. Zhou, R. Dong, R. Devasenathipathy, D.-Y. Wu and L. Yang, Quantification of the Real Plasmonic Field Transverse Distribution in a Nanocavity Using the Vibrational Stark Effect, *J. Phys. Chem. Lett.*, 2023, **14**, 1708–1713.

71 D. T. Kwasnieski, H. Wang and Z. D. Schultz, Alkyl-Nitrile Adlayers as Probes of Plasmonically Induced Electric Fields, *Chem. Sci.*, 2015, **6**, 4484–4494.

72 D. Wright, S. Sangtarash, N. S. Mueller, Q. Lin, H. Sadeghi and J. J. Baumberg, Vibrational Stark Effects: Ionic Influence on Local Fields, *J. Phys. Chem. Lett.*, 2022, **13**, 4905–4911.

73 D. Bhattacharyya, P. E. Videla, M. Cattaneo, V. S. Batista, T. Lian and C. P. Kubiak, Vibrational Stark Shift Spectroscopy of Catalysts under the Influence of Electric Fields at Electrode-Solution Interfaces, *Chem. Sci.*, 2021, **12**, 10131–10149.

74 J. B. Weaver, J. Kozuch, J. M. Kirsh and S. G. Boxer, Nitrile Infrared Intensities Characterize Electric Fields and Hydrogen Bonding in Protic, Aprotic, and Protein Environments, *J. Am. Chem. Soc.*, 2022, **144**, 7562–7567.

75 J. Lee, N. Tallarida, X. Chen, L. Jensen and V. A. Apkarian, Microscopy with a Single-Molecule Scanning Electrometer, *Sci. Adv.*, 2018, **4**, eaat5472.

76 C. Hansch, A. Leo and R. W. Taft, A Survey of Hammett Substituent Constants and Resonance and Field Parameters, *Chem. Rev.*, 1991, **91**, 165–195.

77 R. N. Jones, W. F. Forbes and W. A. Mueller, The Infrared Carbonyl Stretching Bands of Ring Substituted Acetophenones, *Can. J. Chem.*, 1957, **35**, 504–514.

78 P. A. Madden and R. M. Lynden-Bell, Theory of Vibrational Linewidths, *Chem. Phys. Lett.*, 1976, **38**, 163–165.

79 Z. Getahun, C.-Y. Huang, T. Wang, B. De León, W. F. DeGrado and F. Gai, Using Nitrile-Derivatized Amino Acids as Infrared Probes of Local Environment, *J. Am. Chem. Soc.*, 2003, **125**, 405–411.

80 S. Shin, H. Kang, D. Cho, J. Y. Lee and H. Kang, Effect of Electric Field on Condensed-Phase Molecular Systems. II. Stark Effect on the Hydroxyl Stretch Vibration of Ice, *J. Phys. Chem. C*, 2015, **119**, 15596–15603.

81 D. R. Martin and D. V. Matyushov, Why Are Vibrational Lines Narrow in Proteins, *J. Phys. Chem. Lett.*, 2020, **11**, 5932–5937.

82 H.-L. Wang, E.-M. You, R. Panneerselvam, S.-Y. Ding and Z.-Q. Tian, Advances of Surface-Enhanced Raman and IR Spectroscopies: From Nano/Microstructures to Macro-Optical Design, *Light: Sci. Appl.*, 2021, **10**, 161.

83 D. Wright, Q. Lin, D. Berta, T. Földes, A. Wagner, J. Griffiths, C. Readman, E. Rosta, E. Reisner and J. J. Baumberg, Mechanistic Study of an Immobilized Molecular Electrocatalyst by in Situ Gap-Plasmon-Assisted Spectro-Electrochemistry, *Nat. Catal.*, 2021, **4**, 157–163.

84 J. M. Marr and Z. D. Schultz, Imaging Electric Fields in SERS and TERS Using the Vibrational Stark Effect, *J. Phys. Chem. Lett.*, 2013, **4**, 3268–3272.

85 Q. B. Pei, X. X. Zheng, J. J. Tan, Y. Luo and S. J. Ye, Probing the Local Near-Field Intensity of Plasmonic Nanoparticles in the Mid-infrared Spectral Region, *J. Phys. Chem. Lett.*, 2024, **15**, 5390–5396.